AIP Journal of Applied Physics

Nonlinear vibrations of microcantilevers subjected to tip-sample interactions: Theory and experiment

Aidin Delnavaz, S. Nima Mahmoodi, Nader Jalili, M. Mahdi Ahadian, and Hassan Zohoor

Citation: Journal of Applied Physics **106**, 113510 (2009); doi: 10.1063/1.3266000
View online: http://dx.doi.org/10.1063/1.3266000
View Table of Contents: http://scitation.aip.org/content/aip/journal/jap/106/11?ver=pdfcov
Published by the AIP Publishing

Nonlinear vibrations of microcantilevers subjected to tip-sample interactions: Theory and experiment

Aidin Delnavaz,[1] S. Nima Mahmoodi,[2,a)] Nader Jalili,[3] M. Mahdi Ahadian,[4] and Hassan Zohoor[1]
[1]*Center of Excellence in Design, Robotics and Automation (CEDRA), Sharif University of Technology, P.O. Box 11365-9567, Tehran, Iran*
[2]*Center for Vehicle Systems and Safety, Virginia Tech, Blacksburg, Virginia 24061, USA*
[3]*Department of Mechanical and Industrial Engineering, Northeastern University, Boston, Massachusetts 02115, USA*
[4]*Institution for Nanoscience and Nanotechnology (INST), Sharif University of Technology, P.O. Box 14588-89694, Tehran, Iran*

(Received 2 June 2009; accepted 26 October 2009; published online 4 December 2009)

Improvement of microcantilever-based sensors and actuators chiefly depends on their modeling accuracy. Atomic force microscopy (AFM) is the most widespread application of microcantilever beam as a sensor, which is usually influenced by the tip-sample interaction force. Along this line of reasoning, vibration of AFM microcantilever probe is analyzed in this paper, along with analytical and experimental investigation of the influence of the sample interaction force on the microcantilever vibration. Nonlinear integropartial equation of microcantilever vibration subject to the tip-sample interaction is then derived and multiple time scales method is utilized to estimate the tip amplitude while it is vibrating near the sample. A set of experiments is performed using a commercial AFM for both resonance and nonresonance modes, and the results are compared with the theoretical results. Hysteresis, instability and amplitude drop can be identified in the experimental curves inside the particle attraction domain. They are likely related to the interaction force between the tip and sample as well as the ever-present water layer during the experiments. A fair agreement is observed between the theoretical simulations and experimental findings, which obviously demonstrates the effectiveness and applicability of the developed model. © *2009 American Institute of Physics*. [doi:10.1063/1.3266000]

I. INTRODUCTION

Microcantilevers are widely utilized due to their simple structures and effective sensing and actuating capabilities. They have a key role in many scanning probe microscopes. Among them, atomic force microscopes (AFMs) are the most well-known instruments that use microcantilevers. AFM systems are composed of a microcantilever beam equipped with a sharp tip at its free end, capable of revealing the tip-sample interaction forces. As a matter of fact, sample motion generates an interatomic interaction force to the microcantilever tip and influences the static or dynamic responses of the cantilever beam. Both static and dynamic modes can be used in various fields of microcantilever-based sensing and actuating applications.

In this research, the dynamic behavior of a typical AFM's cantilever is investigated. This mode of operation is caused by applying a sinusoidal input motion to the beam support with specific frequency and amplitude. On the other hand, the vibration amplitude of the tip is considered as an output. Microcantilevers in such systems can be simply modeled as a spring with a varying force constant while interacting with the sample. However, it is very important to correctly model this spring as well as its interaction with the sample.

The tip motion in tapping-mode AFM has been analytically and experimentally investigated so far and comparison between continuous and point-mass models has been presented.[1] The microcantilever-sample interaction problem in noncontact AFM has been studied and both lumped-parameters and linear distributed-parameters models of the microcantilever were developed to effectively estimate the interatomic force between the tip and sample.[2] Distributed-parameters modeling of free microcantilever without sample has been linearly analyzed[3] and nonlinearly studied.[4] Moreover, the corresponding frequency response equation has been experimentally verified.[5] Nonlinear dynamics of microcantilever in tapping-mode AFM were also carried out and a comparison between theory and experiment in resonance domain has been reported.[6,7] In addition to flexural vibration, torsional resonance mode AFM under tip-surface interactions has been also studied.[8]

To further explore the vibration behavior of microcantilever beam subject to the tip-sample interaction, it is desirable to develop a reliable model of microcantilever, which enables precise prediction of the vibration amplitude of the tip near the sample. This forms an important step toward designing accurate microcantilever-based sensors and actuators that are applicable in variety of nanoscale imaging systems, nanomanipulators, and nanorobotic arms.

In this paper, a nonlinear distributed-parameters base modeling framework for a microcantilever beam interacting

a)Author to whom correspondence should be addressed. Electronic mail: mahmoodi@vt.edu. Tel.: (540)231-0726.

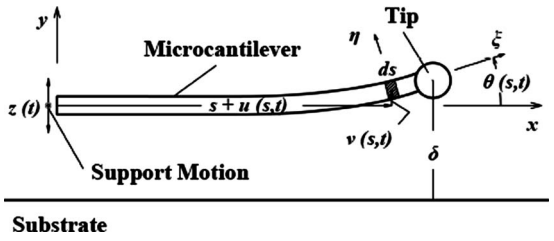

FIG. 1. Schematic representation of microcantilever and sample.

with a sample is developed and experimentally verified. Modulation equations are analytically developed for both resonance and nonresonance cases and compared with the experimental results. The rest of the paper is organized as the follows. In the immediately following section, the mathematical model of the microcantilever beam under tip-sample influence is presented and discussed. Experimental setup and methods are provided in Sec. III. The comparison between theoretical and experimental results is then presented in Sec. IV, followed by summary and concluding remarks in Sec. V.

II. MATHEMATICAL MODEL

In order to obtain the governing equations of motion for the microcantilever beam under the influence of tip-sample interaction, element ds is considered at distance s measured from the beam support in time t while $u(s,t)$ and $v(s,t)$ depict the longitudinal and bending displacements of the microcantilever, respectively (see Fig. 1). It is assumed that Euler–Bernoulli conditions are fully satisfied and the vibration of microcantilever completely lies in two-dimensional plane, as shown in Fig. 1.

The orientation of ds element is presented by angle $\theta(s,t)$. As per Fig. 1, this angle can be calculated by

$$\theta = \arctan\left(\frac{v'}{1+u}\right), \tag{1}$$

where overprime is used to show the derivative with respect to spatial coordinate s. The kinetic and potential energies for single beam element can be obtained as

$$T = \frac{1}{2}m(\dot{u}^2 + \dot{v}^2) + \frac{1}{2}J_\zeta \dot{\theta}^2, \tag{2}$$

$$U = \frac{1}{2}K_\zeta \theta'^2 + \frac{1}{2}E_b A_b \varepsilon_0^2, \tag{3}$$

where J_ζ and K_ζ are microcantilever mass moment and area moment of inertia, respectively. Also overdot represents the derivative with respect to temporal variable t and ε_0 is the Green's strain at neutral axis of the beam section given by

$$\varepsilon_0 = \sqrt{(1+u')^2 + v'^2} - 1. \tag{4}$$

Using Eq. (1) and applying Taylor's series expansion for spatial and temporal derivatives of θ yields,

$$\dot{\theta} = \dot{v}' - \dot{v}'u' - v'^2\dot{v}' - v'\dot{u}', \tag{5}$$

$$\theta' = v'' - v''u' - v'^2 v'' - v'u''. \tag{6}$$

In order to mathematically present the influence of sample on microcantilever vibration, the atomic interaction force is considered as[9]

$$F_{ID} = \frac{H_1}{[\delta + z(t) + v(l)]^2} - \frac{H_2}{[\delta + z(t) + v(l)]^8}, \tag{7}$$

where H_1 and H_2 are Hamaker constants, $z(t)$ is the input displacement at the beam support (see Fig. 1), and δ represents the initial distance between tip and sample, which is also called tip-sample *separation*. Interaction force can then be written by summing up the first six Taylor series terms of Eq. (7) as

$$F_{ID} = K_1 v(l) z(t) + K_2 z(t)^2 + K_3 v(l)^2 + K_4 z(t) + K_5 v(l) + K_6, \tag{8}$$

where

$$K_1 = \frac{6H_1}{\delta^4} - \frac{72H_2}{\delta^{10}}, \tag{9a}$$

$$K_2 = K_3 = \frac{3H_1}{\delta^4} - \frac{36H_2}{\delta^{10}}, \tag{9b}$$

$$K_4 = K_5 = -\frac{2H_1}{\delta^3} + \frac{8H_2}{\delta^9}, \tag{9c}$$

$$K_6 = \frac{H_1}{\delta^2} - \frac{H_2}{\delta^8}. \tag{9d}$$

Considering all the aforementioned derivations, it is now possible to write the Lagrangian function and virtual work expression for the entire system as

$$L = \int_0^l [T + U + \lambda(s)\varepsilon_0] ds, \tag{10}$$

$$\delta W = \int_0^l [m\ddot{z}(t)\delta v - \mu \dot{v}\delta v + f_{ID}\delta v(l)] ds, \tag{11}$$

in which $\lambda(s)$ is the Lagrangian multiplier factor and utilized to handle the inextensibility constraint. Moreover, μ is the beam viscous damping coefficient. For simplicity and representing the equations in a more clear and compact form, the following change of variables is chosen:

$$s^* = \frac{s}{l}, \quad u^* = \frac{u}{l}, \quad v^* = \frac{v}{l}, \quad t^* = t\sqrt{\frac{K_\zeta}{ml^4}},$$
$$\alpha_1 = \frac{J_\zeta}{ml^2}, \quad \alpha_2 = \frac{E_b A_b l^2}{K_\zeta}, \quad \alpha_3 = \mu l^2 \sqrt{\frac{1}{mK_\zeta}}. \tag{12}$$

The Lagrangian function and virtual work are now converted into their nondimensional forms L^* and W^*, respectively, as

$$L^* = \frac{l^2}{K_\zeta} L, \tag{13}$$

$$W^* = \frac{l^2}{K_\zeta} W. \tag{14}$$

Substituting Eqs. (2)–(12) into Eqs. (13) and (14) yields the following expressions for nondimensional Lagrangian function and virtual work expressions, respectively:

$$L = \int_0^1 \left[\begin{pmatrix} \frac{1}{2}\dot{v}^2 + \frac{1}{2}\dot{u}^2 + v''^2 u' \\ + v'' v' u'' - \frac{1}{2} v''^2 + v'^2 v''^2 \end{pmatrix} + \alpha_1 \begin{pmatrix} -\dot{v}'\dot{v}\dot{u}' - v'^2 \dot{v}'^2 \\ -\dot{v}'^2 u' + \frac{1}{2}\dot{v}'^2 \end{pmatrix} + \alpha_2 \begin{pmatrix} -\frac{1}{2} u' v'^2 \\ -\frac{1}{8} v'^4 - \frac{1}{2} u'^2 \end{pmatrix} \right] ds, \tag{15}$$

$$\delta W = \int_0^1 [\ddot{z}(t) - \alpha_3 \dot{v} - \beta_1 z(t) v H(s-1) - \beta_2 z^2(t) - \beta_3 v^2 H(s-1) - \beta_4 z(t) - \beta_5 v H(s-1) - \beta_6] \delta v \, ds. \tag{16}$$

where

$$\beta_i = \frac{l^j K_i}{K_\zeta}, \quad j = \begin{cases} 5 & i = 1,2,3 \\ 4 & i = 4,5 \\ 3 & i = 6 \end{cases} \tag{17}$$

and H is the Heaviside function. The asterisk has been dropped for convenience. So far, there have been two independent generalized coordinates, u and v, to represent the system. It can now be shown that they can be reduced to only one variable by considering the following widely accepted inextensibility assumption

$$\varepsilon_0 \approx u' + \frac{1}{2} v'^2 = 0. \tag{18}$$

The extended Hamilton's principle, $\int_0^t (\delta L + \delta W) dt = 0$, is then applied and inextensibility condition is adopted to derive the single-variable nonlinear integropartial equation of motion

$$\ddot{v} + v'''' + [v'(v'v'')']' + \left[v' \int_1^s \left(\int_0^s v' \dot{v}' ds \right)' ds \right]' + \alpha_3 \dot{v} + \beta_1 v H(s-1) z(t) + \beta_2 z(t)^2 + \beta_3 v^2 H(s-1) + \beta_4 z(t) + \beta_5 v H(s-1) + \beta_6 - \ddot{z}(t) = 0, \tag{19}$$

with the corresponding boundary conditions

$$v(0,t) = 0, \quad v'(0,t) = 0, \quad v''(1,t) = 0, \quad v'''(1,t) = 0. \tag{20}$$

III. FREQUENCY RESPONSE ANALYSIS

The Galerkin's first mode approximation can be utilized in order to discretize Eq. (19) into separate spatial and temporal functions as[10]

$$v(s,t) = \sum_{n=1}^{\infty} C_n(s) q_n(t), \tag{21}$$

in which $q_n(t)$ is the generalized coordinate for nth mode of the beam vibration and $C_n(s)$ is the comparison function appearing in the position-dependent part of the governing equation and can be written in nondimensional form as[10]

$$C_n(s) = \cosh \lambda_n s - \cos \lambda_n s + (\sin \lambda_n s - \sinh \lambda_n s) \frac{\cos \lambda_n + \cosh \lambda_n}{\sin \lambda_n + \sinh \lambda_n}, \tag{22}$$

where $\lambda_n s$ are the roots of the following frequency equation:

$$1 + \cos \lambda_n \cosh \lambda_n = 0. \tag{23}$$

Using the orthogonality of comparison functions, the time-dependent part of the governing equation can be expressed as

$$\gamma_{1n} \ddot{q}_n + \gamma_{2n} q_n + \gamma_{3n} \dot{q}_n + \gamma_{4n} q_n^2 + \gamma_{5n} q_n^3 + \gamma_{6n} q_n^2 \ddot{q}_n + \gamma_{7n} q_n \dot{q}_n^2 + \gamma_{8n} q_n z(t) + \gamma_{9n} \ddot{z}(t) + \gamma_{10n} z(t) + \gamma_{11n} z^2(t) + \gamma_{12n} = 0, \tag{24}$$

where

$$\gamma_{1n} = \int_0^1 C_n^2 ds \tag{25a}$$

$$\gamma_{2n} = \int_0^1 C_n [\beta_5 C_n H(s-1) + C_n''''] ds, \tag{25b}$$

$$\gamma_{3n} = \alpha_3 \int_0^1 C_n^2 ds, \tag{25c}$$

$$\gamma_{4n} = \beta_3 \int_0^1 C_n [C_n^2 H(s-1)] ds, \tag{25d}$$

$$\gamma_{5n} = \int_0^1 C_n (C_n'^2 C_n'''' + 4 C_n' C_n'' C_n''' + C_n''^3) ds, \tag{25e}$$

$$\gamma_{6n} = \gamma_{7n} = \int_0^1 C_n \left(C_n'' \int_1^s \int_0^s C_n'^2 ds ds + C_n' \int_0^s C_n'^2 ds \right) ds, \tag{25f}$$

$$\gamma_{8n} = \beta_1 \int_0^1 C_n [C_n H(s-1)] ds, \tag{25g}$$

$$\gamma_{9n} = -\int_0^1 C_n ds, \tag{25h}$$

$$\gamma_{10n} = \beta_4 \int_0^1 C_n ds, \tag{25i}$$

$$\gamma_{11n} = \beta_2 \int_0^1 C_n ds, \tag{25j}$$

$$\gamma_{12n} = \beta_6 \int_0^1 C_n ds. \tag{25k}$$

Since the comparison functions are orthonormal, Eq. (25a) equals to unity, i.e., $\gamma_{1n}=1$. Also it is assumed that Eq. (25b) equals to square of the linear natural frequency of vibration, i.e., $\gamma_{2n}=\omega_n^2$.

A. Primary resonance response

The method of multiple time scales is chosen to analyze the obtained equation and ϵ is introduced as a book keeping parameter to show infinitesimal quantity in the equation. From this point on, the analysis procedure is divided into two different parts; (i) resonance, and (ii) nonresonance modes. In resonance mode, the frequency of excitation remains near the natural frequency of vibration by the following relation:[11]

$$\Omega = \omega_n + \epsilon\sigma, \tag{26}$$

and the corresponding soft excitation function is given as

$$z(t) = \epsilon z e^{i\Omega t}, \tag{27}$$

in which σ is a detuning parameter to demonstrate how far the frequency of excitation is from natural frequency of vibration. For the resonant case, the ordinary differential equation of motion is generated as

$$\begin{aligned}\ddot{q}_n + \omega_n^2 q_n + \epsilon\gamma_{3n}\dot{q}_n + \epsilon\gamma_{4n}q_n^2 + \epsilon\gamma_{5n}q_n^3 + \epsilon\gamma_6(q_n^2\ddot{q}_n + q_n\dot{q}_n^2) \\ + \epsilon\gamma_8 q_n z(t) + \epsilon\gamma_9\ddot{z}(t) + \epsilon\gamma_{10}z(t) + \epsilon\gamma_{11}z^2(t) + \epsilon\gamma_{12} \\ = 0\end{aligned} \tag{28}$$

According to multiple time scale formulation, the steady-state solution can be expanded as[11,12]

$$q_n(t,\epsilon) = q_{0n}(T_0,T_1) + \epsilon q_{1n}(T_0,T_1) + \cdots, \tag{29}$$

where the two time scales $T_0=t$ and $T_1=\epsilon t$ characterize motions occurring at the linear natural frequency and due to nonlinearities in the system, respectively. Substituting Eq. (29) into Eq. (28) and equating the terms with the same order of ϵ yields

$$\frac{d^2}{dT_0^2}q_{0n} + \omega_n^2 q_{0n} = 0, \tag{30}$$

$$\begin{aligned}\frac{d^2}{dT_0^2}q_{1n} + \omega_n^2 q_{1n} = &-\frac{2d^2}{dT_0 dT_1}q_{0n} - \gamma_{3n}\frac{d}{dT_0}q_{0n} - \gamma_{4n}q_{0n}^2 \\ &- \gamma_{5n}q_{0n}^3 - \gamma_{6n}\left[q_{0n}^2\frac{d^2}{d^2T_0}q_{0n} \right. \\ &\left. + q_{0n}\left(\frac{d}{dT_0}q_{0n}\right)^2\right] - \gamma_{8n}q_{0n}z(t) \\ &+ \gamma_{9n}\omega_n^2\ddot{z}(t) - \gamma_{10n}z(t) - \gamma_{11n}z^2(t) \\ &- \gamma_{12n},\end{aligned} \tag{31}$$

The solution of Eq. (30) is now assumed to be in the following form:

$$q_{0n}(T_0,T_1) = A_n(T_1)e^{i\omega_n T_0} + cc, \tag{32}$$

where A_n is a complex amplitude and cc stands for the complex conjugate of the preceding terms. Substituting Eq. (32) into Eq. (31) gives the following secular terms which are coefficients of $e^{i\omega_n T_0}$, produce time-increasing solutions and ought to be eliminated as a consequence,

$$\begin{aligned}i\left(\gamma_{3n}\omega_n A_n + 2\omega_n\frac{dA_n}{dT_1}\right) + (3\gamma_{5n} - 2\gamma_{6n}\omega_n^2)A_n^2\bar{A} \\ + ze^{i\sigma T_1}(-\gamma_{9n}\omega_n^2 + \gamma_{10n}) = 0.\end{aligned} \tag{33}$$

The complex amplitude A_n can be written in its polar form as

$$A_n = \frac{1}{2}a_n e^{i\phi_n}. \tag{34}$$

If one substitutes Eq. (34) into Eq. (33), the following modulation equation of frequency and amplitude can be obtained

$$\begin{cases}\dfrac{d}{dT_1}a_n(T_1) = -\dfrac{1}{2}a_n\gamma_{3n} + \left(\gamma_{9n}\omega_n - \dfrac{\gamma_{10n}}{\omega_n}\right)z\ sin\ \psi_n, \\ \dfrac{d}{dT_1}\psi_n(T_1) = \sigma + \left(2\gamma_{6n}\omega_n - \dfrac{3\gamma_{5n}}{\omega_n}\right)\dfrac{a_n^2}{8} + \left(\gamma_{9n}\omega_n - \dfrac{\gamma_{10n}}{\omega_n}\right)\dfrac{z}{a_n}\ cos\ \psi_n.\end{cases} \tag{35}$$

in which $\psi_n=-\phi_n+\sigma T_1$. To relate the frequency of excitation or its representative σ to the steady-state amplitude of vibration, the left-hand sides of Eq. (35) are assumed to be zero and ψ_n is eliminated. Thus, the following frequency response equation is extracted:

$$\begin{aligned}(4a_n\gamma_{3n}\omega_n)^2 + [8\sigma a_n\omega_n + a_n^3(2\gamma_{6n}\omega_n^2 - 3\gamma_{5n})]^2 \\ = [8z(\gamma_{9n}\omega_n^2 - \gamma_{10n})]^2.\end{aligned} \tag{36}$$

The solution of the system in resonant case can be finally written as

$$q_n(t) = a_n e^{i(\omega_n t+\phi_n)} + O(\epsilon) = a_n e^{i(\omega_n t+\epsilon\sigma t-\psi_n)} + O(\epsilon)$$
$$= a_n e^{i(\Omega t-\psi_n)} + O(\epsilon). \quad (37)$$

B. Nonresonance response

For nonresonance case, Eq. (24) is regenerated for the hard excitation and ϵ is again introduced to show small-valued terms as[10]

$$\ddot{q}_n + \omega_n^2 q_n + \epsilon\gamma_{3n}\dot{q}_n + \epsilon\gamma_{4n}q_n^2 + \epsilon\gamma_{5n}q_n^3 + \epsilon\gamma_6(q_n^2\ddot{q}_n + q_n\dot{q}_n^2)$$
$$+ \epsilon\gamma_8 q_n z(t) + \gamma_9\ddot{z}(t) + \gamma_{10}z(t) + \gamma_{11}z^2(t) + \epsilon\gamma_{12} = 0. \quad (38)$$

Following the same procedure of resonance case for the nonresonance situation yields

$$\frac{d^2}{dT_0^2}q_{0n} + \omega_n^2 q_{0n} = (\gamma_{9n}\Omega^2 - \gamma_{10n})ze^{i\Omega T_0} - \gamma_{11n}z^2e^{2i\Omega T_0}, \quad (39)$$

$$\frac{d^2}{dT_0^2}q_{1n} + \omega_n^2 q_{1n} = -\frac{2d^2}{dT_0dT_1}q_{0n} - \tilde{\gamma}_{3n}\frac{d}{dT_0}q_{0n} - \gamma_{4n}q_{0n}^2$$
$$- \gamma_{5n}q_{0n}^3 - \gamma_{6n}\begin{pmatrix} q_{0n}^2\dfrac{d^2}{d^2T_0}q_{0n} \\ + q_{0n}\left(\dfrac{d}{dT_0}q_{0n}\right)^2 \end{pmatrix}$$
$$- \gamma_{8n}q_{0n}z(t) - \gamma_{12n}. \quad (40)$$

The solution of Eq. (39) is assumed to be in the form of

$$q_{0n}(T_0,T_1) = A_n(T_1)e^{i\omega_n T_0} + B_n e^{i\Omega T_0} + C_n e^{i2\Omega T_0} + cc, \quad (41)$$

where

$$B_n = \frac{z(4\Omega^2 - \omega_n^2)}{4\Omega^4 - 5\Omega^2\omega_n^2 + \omega_n^4}(-\Omega^2\gamma_{9n} + \gamma_{10n}), \quad (42)$$

$$C_n = \frac{z^2\gamma_{11n}(\Omega^2 - \omega_n^2)}{4\Omega^4 - 5\Omega^2\omega_n^2 + \omega_n^4}. \quad (43)$$

From this equation, it is understood that the amplitude of vibration substantially depends on the difference between the primary resonance frequency and the frequency of excitation as well as the drive amplitude. Substituting Eq. (41) into Eq. (40) yields the following secular term that must be omitted,

$$i\left(\gamma_{3n}\omega_n A_n + 2\omega_n\frac{dA_n}{dT_1}\right) + (3\gamma_{5n} - 2\gamma_{6n}\omega_n^2)A_n^2\bar{A} + (6A_n\gamma_{5n}$$
$$- 2A_n\gamma_{6n}\omega_n^2)(B_n^2 + C_n^2) - 2A_n\gamma_{6n}\Omega^2(B_n^2 + 4C_n^2) = 0. \quad (44)$$

Considering the polar form of the amplitude appeared in Eq. (34) and separating the real and imaginary parts of the equation leads to the following equation which can be called, similar to resonance mode, the modulation equation of frequency and amplitude:

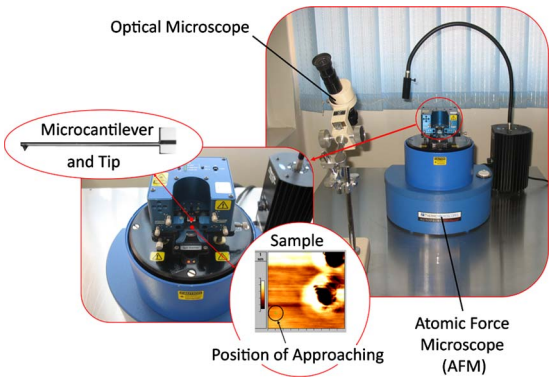

FIG. 2. (Color online) Experimental setup.

$$\begin{cases} \dfrac{d}{dT_1}a_n(T_1) = -\dfrac{1}{2}a_n\gamma_{3n} \\ \dfrac{d}{dT_1}\phi_n(T_1) = -\dfrac{1}{8\omega_n}\begin{pmatrix} a_n^2(-3\gamma_{5n} + 2\gamma_{6n}\omega_n^2) + \\ 8\gamma_{6n}\Omega^2(B_n^2 + 4C_n^2) \\ + (-24\gamma_{5n} + 8\gamma_{6n})(B_n^2 + C_n^2) \end{pmatrix} \end{cases}. \quad (45)$$

The solution of Eq. (38) eventually reduces to

$$q_n(t) = a_n e^{i(\omega_n t+\phi_n)} + B_n e^{i\Omega t} + C_n e^{i2\Omega t} + O(\epsilon). \quad (46)$$

The first term decays with time, while the second and third terms do not. The former is the transient solution and the latter is steady-state or particular solution. This is exactly the same as in the case of forced vibration of linear systems.

IV. EXPERIMENTAL SETUP AND METHODS

The validity of the developed equations of motion is examined experimentally in this section, and the effects of the tip-sample interaction on the amplitude of microcantilevers' vibration are extensively studied. The experimental setup, shown in Fig. 2, consists of an *Auto-probe CP-Research* system of AFM fabricated by *TM Microscopes Veeco Metrology Group*®. It is equipped with 20× optical microscope for the preliminary adjustments, pneumatic vibration-free table, point lighting source and the computer system to automatically control the setup. The experimental setup is first calibrated by the factory-defined instructions and the target experiments are then run in the atmospheric condition. Each experimental run includes the following successive steps.

(1) Microcantilever and sample are carefully installed on the system.
(2) Microcantilever tip vibration is measured by the laser system. In this system, a laser beam is steered to reach the end of microcantilever on top of the tip and the reflected laser beam is aligned to the center of position sensitive photodetector (PSPD) before the experiment starts. PSPD collects the reflected laser beams and converts them to electric signals for further processing in the computer.

TABLE I. Microcantilever parameters.

Microcantilever			
Type	MPP-3120-cont20 Metrology Probes		
Shape	Rectangular		
Material	Si doped with P, a ±40 nm of Al has been coated on one side		
	Range	Nominal Values	Simulated Values
Length (μm)	440–450	450	450
Width (μm)	30–40	35	30
Thickness (μm)	3.5–4.5	4	3.5
Frequency (kHz)	13–40	20	30
Force Constant (N/m)	0.45–18	0.9	0.9
Density (kg/m^3)	⋯	⋯	2330
Viscose damping (Ns/m)	⋯	⋯	0.0001
Tip			
Tip Height (μm)	15–20	⋯	⋯
Front Angle		15°	⋯
Side Angle		17.5°	⋯
Tip Radius (nm)	<12.5	<10	⋯
Tip Set Back (μm)	5–25	15	⋯

(3) Noncontact mode of AFM is run and the substrate is thoroughly scanned in order to find a suitable place with desirable nearly flat area.
(4) The microcantilever tip is located at top of this flat area and the experiment starts.
(5) When the microcantilever is away from the surface, the frequency response curve (FRC) is plotted and the resonant peaks are obtained. The drive frequency is then chosen in such a way that dominates the resonance or nonresonance conditions as demanded.
(6) The microcantilever is approaching to and retracting from the sample and spectroscopy toolbox is used to generate the plot of vibration amplitude versus tip-sample vertical distance.
(7) The last step is repeated for many times to inspect the repeatability, guarantee the validity of acquired data and eliminate the statistical errors.

V. THEORETICAL AND EXPERIMENTAL RESULTS COMPARISON

The equation of vibration amplitude has been derived for resonance and non-resonance modes separately, along with an experimental AFM setup to perform relevant experiments in the preceding sections. The FRC of microcantilever beam with the properties listed in Table I is depicted in Fig. 3 in which the primary resonance frequency is clearly recognized at $f=30450$ Hz.

There are some uncertainties for the properties of microcantilever beam given in Table I. Some of these uncertainties are declared by the manufacturer as well and are limited to the specified range. They mainly appear in the geometrical dimensions and the material properties of the beam. One can search inside the uncertainties' ranges in order to find the values for which the theoretical resonance frequency can best fit the experimental resonance frequency as seen in Fig. 3.

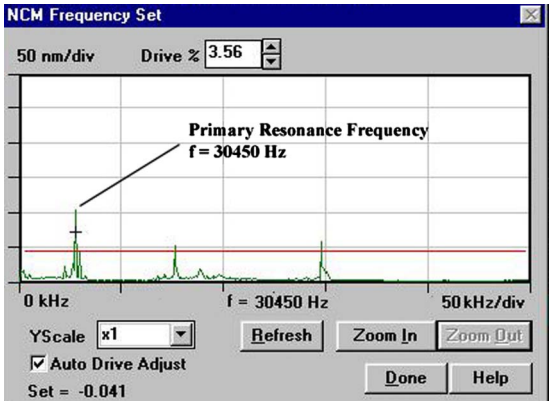

FIG. 3. (Color online) Frequency response curve of microcantilever.

These values are shown in "simulated values" column of Table I and will be later used instead of "nominal values" to analytically calculate the amplitude of vibration.

In order to experimentally verify the obtained equation of motion and the corresponding amplitude-distance equations, different frequencies and amplitudes are applied as an input motion to the specified microcantilever beam. Low amplitude of excitation with the frequency near the first harmonic of motion signifies the soft resonance mode. Conversely, high amplitude of input signal with the frequency away from the primary resonance frequency characterizes the hard nonresonance mode. In the soft resonance mode, the experiment is done once for the frequencies very close to the primary resonance frequency and once repeated for the frequencies a little farther. The former is called small-σ resonant mode, while the latter is called large-σ resonant mode.

The target frequencies and amplitudes for which experimental data are gathered and theoretical formulations are numerically simulated are presented in Table II. As illustrated in Table II, in the resonance mode, it is assumed that the frequency of excitation is just a little away from the first harmonic of motion; that is, 0.1% for small-σ and 2.5% for large-σ. Again, the frequency of excitation is chosen to be completely far away from the primary resonance frequency in order to fulfill the nonresonant situations.

Figure 4 demonstrates the experimental results and the theoretical simulation of vibration amplitude with respect to the tip-sample separation for small-σ resonant mode. For the experimental results, there are two separate curves: approaching and retracting. The first one depicts the behavior of the beam while the tip goes toward the sample and the second one shows the situation in which the tip comes back from the sample. There is a large gap between the approaching and retracting curves, which is called *hysteresis* and will

TABLE II. Experiment data.

	Resonant small-σ	Resonant large-σ	Nonresonant
Natural frequency (Hz)	30 450	30 450	30 450
Excitation frequency (Hz)	30 480	31220	110 510
σ (Hz)	+30	+770	⋯
Excitation amplitude (nm)	~10	~10	~100

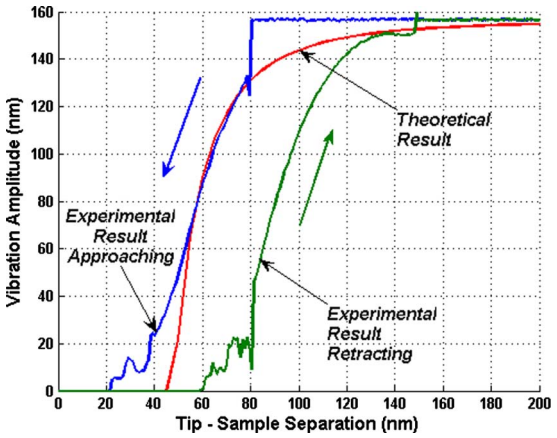

FIG. 4. (Color online) Vibration amplitude vs tip-sample separation; resonant small-σ condition.

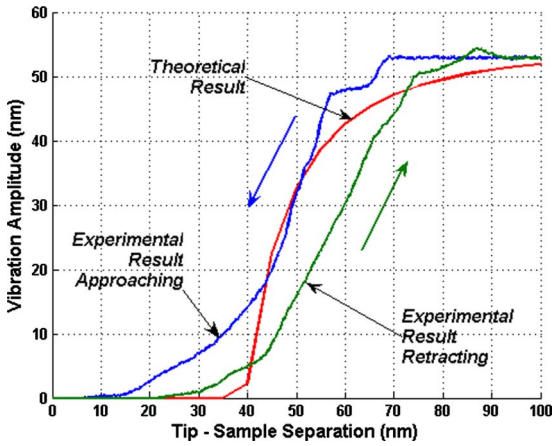

FIG. 5. (Color online) Vibration amplitude vs tip-sample separation; resonant large-σ condition.

be discussed later. For all the curves, there is also a special region in which the amplitude of vibration changes with the tip-sample distance and is called the *sample attraction region*. Outside of this region, the amplitude of vibration remains constant despite of changing the tip-sample distance.

It should be clarified that the initial conditions of obtained equation are set to zero during the simulation and consequently, the theoretical curve must be compared with the experimental approaching curve for which these initial conditions are fully satisfied.

When Fig. 4 is scrutinized, it is unveiled that there is an unstable region in the amplitude of the beam vibration very close to the sample, i.e., when δ has very small value. The unstable region may be a consequence of remarkable increasing in the attraction force near the sample. This interatomic interaction force prevents the beam from vibrating and makes it eventually stop its motion and stick to the surface. In addition to instability region, there is a sudden change in the amplitude of vibration at the point in which the tip enters the sample attraction domain. As a matter of fact, the tip is suddenly absorbed by the sample at the border of attraction region and it is followed by drop. The unstable region can be well predicted by the theoretical model where the square of natural frequency equals to negative values and loses its meaning. However, sudden changes in the amplitude cannot be theoretically identified at all. Outside the sample attraction region, approaching and retracting curves approach each other, and the theoretical curve is well fitted with the experimental one.

By choosing the frequency of excitation a little bit away from the natural frequency of vibration, σ possesses larger value and becomes more comparable with the primary resonance frequency. Although Eq. (36) is still valid for large-σ, the result is not as satisfactory as small-σ situation. Moreover, by increasing the detuning parameter, instability and dropping phenomena are gradually weakening. The theoretical and experimental results for large-σ are represented in Fig. 5.

For nonresonant case, it is assumed that the frequency of excitation is at a far distance from the primary resonance such that Eq. (36) is no longer valid, and instead, Eqs. (42) and (43) must be substituted. The results for this situation are illustrated in Fig. 6. A great drop in the amplitude values and a large hysteresis between approaching and retracting curves can be vividly recognized in nonresonant mode (see Fig. 6).

The hysteresis and amplitude drop can be attributed to the thin film of water confined between the tip and a solid surface. These experiments are carried out in free atmosphere without any special considerations. Therefore, condensing the water vapors, which typically exist in the laboratory atmosphere, on the surface of all materials is hence a valid assumption. This condensed water layer produces an extra interatomic force, which is called capillary force and influences the tip vibration.[8] In other words, the severe hysteresis in the curves and a sudden drop in the amplitude values can be considered as a signature of water layer presence like what has been reported in other similar experiments.[13–15]

VI. CONCLUSIONS

Microcantilever vibration subject to the tip-sample interaction was studied in this paper and the amplitude of vibration for different tip-sample distance (σ) was analytically and experimentally investigated. The findings were divided

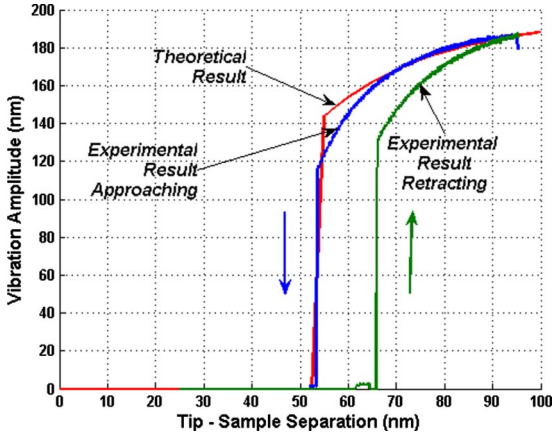

FIG. 6. (Color online) Vibration amplitude vs tip-sample separation; nonresonant condition.

into two major groups: resonance and non-resonance modes. Resonant experiments were also carried out once for the small σ and again for the large σ.

In all experimental results, inside the sample attraction region, a hysteresis between approaching and retracting curves was observed. However, these two curves joined outside the attraction region and remained constant. For small σ, there were clear unstable motion and falling trend at both ends of the sample attraction region. Unstable region can be perfectly tracked by the theoretical model, while the falling region cannot. For larger σ, the developed resonance model was persistently valid and unexpected behaviors like instability and dropping could be hardly detected. In non-resonance situation, the hysteresis between approaching and retracting curves was amplified and the amplitude of vibration suddenly and considerably dropped. Hysteresis and other unexpected changes in the curves may originate from the existence of water layer on the sample during the experiment. Considering both theoretical and experimental results, it was concluded that the developed theoretical models can reasonably match with the real behavior of microcantilever vibration.

ACKNOWLEDGMENT

The authors are indebted to Professor A. Iraji-zad and ESCA Laboratory personnel from Department of Physics at Sharif University of Technology for their great supports in experimental setups and validation.

[1]T. R. Rodriguez and R. Garcia, Appl. Phys. Lett. **80**, 1646 (2002).
[2]N. Jalili, M. Dadfarnia, and D. M. Dawson, ASME J. Dyn. Syst., Meas., Control **126**, 327 (2004).
[3]S. Barhen, Phys. Lett. A **372**, 947 (2007).
[4]S. N. Mahmoodi and N. Jalili, Int. J. Non-Linear Mech. **42**, 577 (2007).
[5]S. N. Mahmoodi, N. Jalili, and S. Khadem, J. Sound Vib. **311**, 1409 (2007).
[6]Y. Zhang and Y. Zhao, Chaos, Solitons Fractals **34**, 1021 (2007).
[7]S. I. Lee, S. W. Howell, A. Raman, and R. Reifenberger, Phys. Rev. B **66**, 115409 (2002).
[8]L. Huang and C. Su, Ultramicroscopy **100**, 277 (2004).
[9]Q. Q. Hu and L. Q. Chen, Chaos, Solitons Fractals **36**, 740 (2006).
[10]A. H. Nayfeh and D. T. Mook, *Nonlinear Oscillations* (Wiley, New York, 1979).
[11]A. H. Nayfeh, *Perturbation Methods* (Wiley, New York, 1973).
[12]A. H. Nayfeh, *Nonlinear Interactions* (Wiley, New York, 2000).
[13]R. Brunner, O. Marti, and O. Hollricher, J. Appl. Phys. **86**, 7100 (1999).
[14]L. Vaccaro, M.-P. Bernal, F. Marguis-Weible, and C. Duschl, Appl. Phys. Lett. **78**, 3110 (2000).
[15]M. Antognozzi, A. D. L. Humphris, and M. J. Miles, Appl. Phys. Lett. **78**, 300 (2001).